This is an *Accepted Manuscript*, which has been through the Royal Society of Chemistry peer review process and has been accepted for publication.

Accepted Manuscripts are published online shortly after acceptance, before technical editing, formatting and proof reading. Using this free service, authors can make their results available to the community, in citable form, before we publish the edited article. We will replace this *Accepted Manuscript* with the edited and formatted *Advance Article* as soon as it is available.

You can find more information about *Accepted Manuscripts* in the **Information for Authors**.

Please note that technical editing may introduce minor changes to the text and/or graphics, which may alter content. The journal's standard **Terms & Conditions** and the **Ethical guidelines** still apply. In no event shall the Royal Society of Chemistry be held responsible for any errors or omissions in this *Accepted Manuscript* or any consequences arising from the use of any information it contains.

Synergetic effect of Zn substitution on the electron and phonon transport in $Mg_2Si_{0.5}Sn_{0.5}$ based thermoelectric materials

Hongli Gao[a,b], Tiejun Zhu[a], Xinbing Zhao[a], Yuan Deng[b*]*

[a] State Key Laboratory of Silicon Materials and Department of Materials Science and Engineering, Zhejiang University, Hangzhou, 310027, China.

[b] School of Materials Science and Engineering, BeiHang University, Beijing, 100191, China.

[*]To whom correspondence should be addressed.

E-mail: zhaoxb@zju.edu.cn; dengyuan@buaa.edu.cn

Abstract:

$Mg_2Si_{1-x}Sn_x$ alloys are the perspective material for thermoelectric generators at moderate temperature. The thermoelectric properties of $Mg_2Si_{0.5}Sn_{0.5}$ based thermoelectric materials with only Zn substitution and Zn, Sb co-doping were investigated. Isoelectronic Zn substitution did not affect the carrier concentration but improved the carrier mobility. Zn atom incorporated into a Sb-doped $Mg_2Si_{0.5}Sn_{0.5}$ matrix simultaneously boosted the power factor and suppressed the lattice thermal conductivity, leading to an enhancement of the thermoelectric figure of merit ZT of the resulting bulk materials. The interplay between the electron and phonon transport of $Mg_2Si_{0.5}Sn_{0.49}Sb_{0.01}$ substituted with Zn at Mg site results in an enhancement of the ZT by 25% at ~ 730 K, from $ZT \approx 0.8$ in $Mg_2Si_{0.5}Sn_{0.49}Sb_{0.01}$ to $ZT \approx 1.0$ in $Mg_{1.98}Zn_{0.02}Si_{0.5}Sn_{0.49}Sb_{0.01}$. Solid solutions in the Mg_2Si-Mg_2Sn system appear more promising for thermoelectric applications.

Introduction

Thermoelectric convertors (TEC) who can recover the waste heat from the exhaust of an automotive engine are a very attractive way for a reduction of the fuel consumption. TECs with high overall efficiency directly convert heat into electricity without moving parts and thus, not only decrease our reliance on fossil fuels but also actively counteract global warming [1]. Thermoelectric (TE) materials act an important role in this process. Thermoelectric performance is characterized by a dimensionless figure of merit [1], $ZT=(\alpha^2\sigma/\kappa)T$, where σ is the electrical conductivity, α the Seebeck coefficient, T Kelvin temperature, and $\kappa=\kappa_L+\kappa_e$ the thermal conductivity, which as normal is written as a sum of lattice and electronic contributions. Improvement and optimization of the thermoelectric efficiency require control and manipulation of electronic and thermal properties, and this has long been elusive. Much endeavor has been put into the investigation of high performance TE materials [2-6], aiming at increasing the thermoelectric figure of merit by maximizing the power factor ($PF=\alpha^2\sigma$) and/or minimizing the thermal conductivity. Recently, nanostructuring [7,8] and band engineering [9,10] have been proved to be efficient ways to achieve improved thermoelectric performance. However, since σ, α, and κ_e are entwined by the carrier concentration, it is rather challenging to achieve power factor enhancement and thermal conductivity reduction simultaneously.

Mg$_2$(Si,Sn) based solid solutions have recently attracted much attention [11-13] because of their abundantly available and environment-benign constituent elements, and the promising TE performance with a $ZT\approx1.0$ at 800 K. It has been reported that in n-type Mg$_2$(Si,Sn) the electron donor dopants, such as Sb [11,14-17] and Bi [18] at the Si site and La [19]

and Al [20] at the Mg site, improve the *ZT* of materials significantly, with major contribution due to the optimization of power factor. Furthermore, band convergence [13,21] is an effective strategy for enhancing thermoelectric properties, which gives rise to large values of the Seebeck coefficient with no adverse effect on the carrier mobility. With regard to the thermal conductivity reduction, formation of solid solution, natural nanostructure [12] and vacancy at the Mg site [22,23] provide effective phonon-scattering centers. Over all, power factor optimization can be achieved by tuning carrier concentration or band convergence, but carrier concentration increase always leads to mobility sacrifice and band convergence only occurs at certain Si/Sn ratio [13]. Thus it is meaningful to develop a strategy to partially decouple the negative correlation between carrier concentration and mobility.

Herein, in $Mg_2Si_{0.5}Sn_{0.5}$ based thermoelectric materials, Zn was selected as the isoelectronic substitution atom to perform this task. According to the KKR-CPA electronic structure calculations [24], Zn preferentially occupies the Mg site. By means of Zn substitution at the Mg site although no extra charge is introduced into the disordered system, a modulation in the material's band structure may be expected due to lattice expansion. In the research of ZnO semiconductor materials [25], Group II elements (Cd, Mg) are usually selected as doping agent to modulate the value of the band gap and increase the intensity of UV emission. Mg substitutes into ZnO lattice at Zn site, leading to the band gap increase. Conversely, it is rational to anticipate similar effect of Zn substitution at the Mg site in $Mg_2(Si,Sn)$ solid solutions. Besides, owing to the mass and size difference between Mg and Zn atoms, isoelectronic substitution will introduce mass fluctuation scattering and strain field fluctuation scattering for phonons. Zn substitution is

expected to improve the thermoelectric properties of the Mg_2Si-Mg_2Sn solid solutions.

In this paper we have focused on the correlation of the thermoelectric transport properties of Zn substituted $Mg_2Si_{0.5}Sn_{0.5}$ based thermoelectric materials with variable dopant concentration. $Mg_2Si_{0.5}Sn_{0.5}$ based compounds with only Zn substitution and Zn+Sb co-doping were synthesized，and the thermoelectric properties of these samples were investigated and carefully analyzed.

Experimental

$Mg_{2-x}Zn_xSi_{0.5}Sn_{0.5}$ ($x = 0$, 0.005, 0.01) and $Mg_{2-y}Zn_ySi_{0.5}Sn_{0.49}Sb_{0.01}$ ($y = 0$, 0.01, 0.02, 0.06) ingots were prepared by direct reaction of the constituent elements in fused tantalum ampoules. In addition to the stoichiometric quantities of Mg, Si, Sn, Zn, Sb powders (Alfa Aesar), a sufficient amount of additional Mg powder was added to compensate for the evaporation of Mg during the heat treatment. The ampoule were heated and kept at 650 ^oC for 2 h, 1100 ^oC for 10 h, cooled down naturally afterwards. In order to obtain the dense and regular-shaped bulk samples without cracks, the alloy ingots were ground and sieved to ~50 mm and hot-pressed in a graphite die of Φ12.7 mm under a pressure of 80 MPa at 993 K for 2 h. The relative densities of all the pressed pellets are of >99%.

Room temperature XRD patterns were taken on a Rigaku-D/MAX-2550PC diffractometer with Cu K_α radiation. The electrical conductivity σ and Seebeck coefficient α were measured in the temperature range between 300 K and 723 K on a computer-aided apparatus under vacuum using a direct-current (DC) four-probe method and differential voltage/temperature technique, respectively. The thermal conductivity was calculated by using $\kappa = D\rho_DC_P$, where ρ_D is the sample density estimated by an

ordinary dimensional and weight measurement procedure. Thermal diffusivity D and specific heat C_P were measured by a laser flash method on a Netzsch LFA457 with a Pyroceram9606 standard. The Hall coefficient, R_H, measurements were performed at 300 K on a Quantum Design PPMS-9T using a four-probe configuration, with the magnetic field sweeping between ±4.0 T. Then the carrier concentration n and Hall mobility μ_H were calculated using $n=-(1/eR_H)$ and $\mu_H=\sigma R_H$, respectively.

Results and discussion

X-ray diffraction patterns

As-hot-pressed pellets of $Mg_{2-x}Zn_xSi_{0.5}Sn_{0.5}$ (x = 0, 0.005, 0.01) and $Mg_{2-y}Zn_ySi_{0.5}Sn_{0.49}Sb_{0.01}$ (y = 0, 0.01, 0.02, 0.06) samples were fabricated and the X-ray diffraction (XRD) patterns are shown in Fig. 1. The XRD shows that the Zn-substituted materials contain mostly one phase and have an *Fm-3m* structure similar to the parent material. All sintered samples show clear Bragg peaks from an anti-fluorite-type structure (space group, *Fm-3m*) with the diffraction peaks locating between the major peaks of pure Mg_2Si and Mg_2Sn. These results imply the formation of $Mg_2Si_{1-x}Sn_x$ solid solutions.

Electronic transport

The temperature dependences of electrical transport properties of $Mg_{2-x}Zn_xSi_{0.5}Sn_{0.5}$ and $Mg_{2-y}Zn_ySi_{0.5}Sn_{0.49}Sb_{0.01}$ samples are shown in Fig. 2. For only Zn doping (as denoted by the hollow symbols), all samples indicate typical semiconducting behavior, the electrical conductivity increases monotonically with temperature between 300 K and 730 K, while the Seebeck coefficients firstly increase and then decrease with increasing temperature. Temperature causes electrons to be promoted to the conduction band. The dependence of conductivity on temperature is like other thermally activated processes [1, 26]:

$$\sigma = A\exp(-\frac{E_g}{2k_BT}) \tag{1}$$

where A is a constant, E_g the band gap energy, k_B the Boltzmann constant, T the Kelvin temperature. For an intrinsic semiconductor, plotting $\ln\sigma$ vs $1/T$ produces a straight line of slope $E_g/2k_B$ from which the band gap energy E_g can be determined. The calculated energy gap of the undoped $Mg_2Si_{0.5}Sn_{0.5}$ sample is about 0.6 eV. It has been reported that the energy gaps of Mg_2Si and Mg_2Sn are 0.77 eV and 0.35 eV respectively [27]. The calculated E_g of pristine $Mg_2Si_{0.5}Sn_{0.5}$ sample is close to the average energy gap of Mg_2Si and Mg_2Sn of 0.56 eV, implying the composition is close the nominal one. The room temperature carrier concentration which varies in the range of $2.3\sim2.7\times10^{18}$ cm^{-3} was measured. The number of the outermost electron of Mg and Zn atom are both 2. Consequently it is reasonable to propose that the substitution of Zn for Mg will not lead to the increase of carrier concentration, which is consistent with the experimental results.

From the phenomena observed above, we can deduce that the Zn substitution has little effect on the thermoelectric properties of $Mg_2Si_{0.5}Sn_{0.5}$ based materials. We speculate that the carrier concentration might be too low to manifest the function of Zn atoms. Based on this hypothesis, $Mg_2Si_{0.5}Sn_{0.5}$ based materials with higher carrier concentrations were obtained by Sb doping and the effect of Zn substitution were investigated.

Temperature dependences of electrical transport properties of as-hot-pressed pellets of $Mg_{2-y}Zn_ySi_{0.5}Sn_{0.49}Sb_{0.01}$ samples (with Zn, Sb co-doping) were also plotted in Fig. 2 (as denoted by the solid symbols). The temperature dependence of the electrical conductivity (Fig .2(a)) is typical of degenerate semiconductors where the decrease of the electrical conductivity with temperature is mostly associated with an increase in carrier

scattering by phonons. The electrical conductivity of the sample with Sb=0.01/Zn=0 firstly decreases and then stabilizes with the increase of temperature. In Fig. 2(b), the Seebeck coefficient was negative within the whole temperature range, with increasing temperature dependence. From Fig. 2, we can calculate the power factors (*PF*) of the $Mg_2Si_{0.5}Sn_{0.5}$ and $Mg_{2-y}Zn_ySi_{0.5}Sn_{0.49}Sb_{0.01}$ samples. At 740 K, *PF* of the sample with Sb=0.01/Zn=0.02 is $\approx 3.2\times10^{-3}$ $Wm^{-1}K^{-2}$, which is ten times higher than $PF\approx0.3\times10^{-3}$ $Wm^{-1}K^{-2}$ for samples with only Zn substitution and also 33% higher than $PF\approx2.4\times10^{-3}$ $Wm^{-1}K^{-2}$ of Sb=0.01/Zn=0 sample.

Hence the most intriguing question is how Zn or Sb enhances the thermoelectric properties and how this enhancement may be related to their electronic states. In order to elucidate how the Zn-corporation affects the TE properties, we further investigated the room temperature physical properties of the $Mg_{2-y}Zn_ySi_{0.5}Sn_{0.49}Sb_{0.01}$ samples.

Fig. 3 depicts the room temperature carrier concentration and mobility of the $Mg_{2-y}Zn_ySi_{0.5}Sn_{0.49}Sb_{0.01}$ samples. There is little variation of the carrier concentration with the change of Zn content, which is around 2.4×10^{20} cm^{-3}. This phenomenon is consistent with the results we got for the samples with only Zn substitution, which is owing to the fact that the number of the outermost electron of Mg and Zn atom are the same. The mobility was obtained according to the relationship $\sigma=ne\mu_H$. The mobility monotonically increases with the increase of Zn content. When the mobility of "free electrons" is dominated by the phonon, the mobility can be described as [28]

$$\mu_H = \frac{2^{1/3}k_Bhe}{3(2\pi)^2}\frac{\theta_D^2 M}{am^{*2}C^2}\frac{1}{Tn^{1/3}} \tag{2}$$

where *h* is the Plank constant, θ_D is the Debye temperature, *M* is the average atomic weight, *a* is the average interatomic distance, *m** is the effective mass, and *C* relates to

the phonon electron coupling and is expected to be on the order of 1-10 eV. From

Equation (2) we can deduce that the increase of μ_H may be ascribed to the increase of θ_D,

M or the decrease of a, m^*, n. The ive atomic mass of Mg and Zn are 24.305 and 65.38,

respectively. For $Mg_{2-y}Zn_ySi_{0.5}Sn_{0.49}Sb_{0.01}$ samples, M increases as Zn content increases,

leading to a higher mobility.

For good thermoelectric materials, high power factor and low thermal conductivity

are favorable to get higher ZT. It is well known that formation of solid solutions is

desirable for thermoelectrics due to their lower thermal conductivities [1]. The reduction of

lattice thermal conductivity by alloying has been compensated by the counter effect of the

reduced carrier mobility. The Zn substitution method we proposed here compensated the

mobility loss, which provides another way to improve the thermoelectric properties.

According to the Boltzmann transport equations (within the single parabolic band

assumption) [1], the Seebeck coefficient α and the carrier concentration n are given by

$$\alpha = \mp \left(\frac{k_B}{e}\right)\left[\frac{r+2}{r+1}\frac{F_{r+1}(\xi)}{F_r(\xi)} - \xi\right] \tag{3}$$

$$n = \frac{4}{\sqrt{\pi}}\left(\frac{2\pi m^* k_B T}{h^2}\right)^{3/2} F_{1/2}(\eta_F) \tag{4}$$

with the Fermi integrals $F_i(\eta)$ defined by

$$F_i(\eta_F) = \int_0^\infty \frac{x^i dx}{1+e^{(x-\eta_F)}} \tag{5}$$

Where r is scattering factor, k_B the Boltzman's constant; e the electron charge,

$F_r(\xi)$ the Fermi integration, and ξ the reduced Fermi energy ($\zeta/k_B T$).

As shown in Fig. 4, the carrier concentration dependence of the Seebeck coefficient

follows roughly the single parabolic band line at room temperature. The solid line in Fig.

4 is generated using $r=0$, and an effective mass of $m^*=2.3m_0$ (m_0 is the electron mass) at room temperature, which is consistent with previously reported values [11]. When the carrier concentration is low, the effective mass locates around low m^*/m_0 (≈ 1.0). While the carrier concentration goes higher, the effective mass moves to $m^*/m_0=2.3$. At the same carrier concentration, when the effective mass is higher, the Seebeck coefficient is higher. The electron effective mass of Mg_2Si and Mg_2Sn are $0.5m_0$, $1.2m_0$ respectively [1]. According to the band structure calculation for Mg_2Si and Mg_2Sn near Fermi level [29], the conduction band minimum is created from different states for Mg_2Si and Mg_2Sn. For Mg_2Si it is created from Si states and for Mg_2Sn it is created from Mg states. So, the positions of these minima should be changed in the solid solutions. In $Mg_2Si_{1-x}Sn_x$ solid solutions, the two conduction bands converge as the content of Sn increases [13]. The resulting increased valley degeneracy leads to a significantly enhanced density-of-states effective mass.

Thermal transport

Fig. 5 displays the thermal transport properties of the $Mg_{2-y}Zn_ySi_{0.5}Sn_{0.49}Sb_{0.01}$ samples. In Fig. 5(a), the total thermal conductivity all decreases with the increase of temperature. The total thermal conductivity is the sum of a lattice component, κ_L, due to propagation and carrier component, κ_e, due to heat transported by charge carriers. The carrier component κ_e, reflecting the contribution of the carriers in the heat conduction process, is quantified through the Wiendemann-Franz law, which simply states that $\kappa_e=L\sigma T$, where L is the Lorenz number. The Lorenz number L on the basis of Fermi-Dirac statistics is as follows:

$$L = \left(\frac{k_B}{e}\right)^2 \left[\frac{r+3}{r+1} \frac{F_{r+2}(\xi)}{F_r(\xi)} - \left\{ \frac{r+2}{r+1} \frac{F_{r+1}(\xi)}{F_r(\xi)} \right\}^2 \right] \tag{6}$$

L was estimated by equation (6) for the acoustic phonon scattering of r=0 and Fermi energy ξ was calculated by the equation (3) using the measured α. Lattice thermal conductivity was calculated according the equation $\kappa_L = \kappa - L\sigma T$ and presented in Fig. 5(c). The calculated L values (Fig. 5(b)) decrease with the increase of temperature for all samples due to decreasing ξ. L for all the samples are lower than the degenerate limit 2.45×10^{-8} V^2K^{-2}. In Fig. 5(c), the lattice thermal conductivity of all the samples monotonically decrease with temperature, but still much higher than the theoretical minimum lattice thermal conductivity $\kappa_{L\text{-min}}$ calculated by Cahill's formulation [30, 31]. In general high temperature lattice thermal conductivity is sensitive to the point-defect scattering. The lattice thermal conductivity decreases with the increase of Zn content, which is much lower than the sample with only higher Sb doping [14] (dashed line). Isoelectronic substitution introduces mass fluctuation scattering and strain field fluctuation scattering for phonons due to the mass and size difference between alloying atoms and host atoms [32].

With the average inter-atomic spacing and the velocity of sound known, we estimated the minimum lattice thermal conductivity κ_{min} of $Mg_2Si_{0.4}Sn_{0.6}$ and plotted it in Fig. 5(c) as a function of temperature. The minimum lattice thermal conductivity was calculated by equation (7). The thermal conductivity resulting from the random walk between these localized quantum mechanical oscillators can then be written as the following sum of three Debye integrals [30].

$$\kappa_{\min} = \left(\frac{\pi}{6}\right)^{1/3} k_B n_a^{2/3} 3 v_s \left(\frac{T}{\theta_i}\right)^2 \int_0^{\theta_i/T} \frac{x^3 e^x}{\left(e^x - 1\right)^2} dx \qquad (7)$$

The sum is taken over the three sound modes (two transverse and one longitudinal) with speeds of sound v_i; θ_i is the cutoff frequency for each polarization expressed in degrees K, $\theta_i = v_i\left(h/2\pi k_B\right)\left(6\pi^2 n_a\right)^{1/3}$ and n_a is the number density of atoms. For $Mg_2Si_{0.4}Sn_{0.6}$, the speed of sound v_i is 4101 m/s according to reference [12, 13].

Figure of merit

The temperature dependent dimensionless figure of merit ZT was calculated and shown in Fig. 6(a). The ZT of samples with Zn, Sb co-doping are improved compared to that of pristine $Mg_2Si_{0.5}Sn_{0.5}$ compound. A $ZT_{\max} \approx 1.0$ was obtained at ~ 740 K for $Mg_{1.98}Zn_{0.02}Si_{0.5}Sn_{0.49}Sb_{0.01}$, which is quite comparable with those of the state-of-the-art PbTe based thermoelectric alloys operated in the intermediate temperature range. The Fig. 6(b) shows experimentally determined ZT values at a temperature of 750 K plotted as a function of carrier concentration. The modeled ZT values were generated using an effective mass of $2.3m_0$, an intrinsic mobility of 15 $cm^2V^{-1}s^{-1}$ and a lattice thermal conductivity of 1.5 $Wm^{-1}K^{-1}$.Good agreement is found with the Single parabolic band model (solid line). This research provides a method to enhance the power factor and ZT values, which should be helpful for further optimization of ZT values in $Mg_2Si_{1-x}Sn_x$ compounds.

Conclusions

In this paper, Zn substituted $Mg_2Si_{0.5}Sn_{0.5}$ based thermoelectric materials with variable dopant concentration were synthesized by tantalum-tube weld melting method followed by hot pressing and the thermoelectric transport properties of them were

investigated in detail. Zn substitution introduced no extra charge, and didn't change the carrier concentration. However, as the carrier concentration was increased by Sb doping, Zn substitution improved the electron mobility dramatically from 23 (y=0) to 42 (y=0.02) $cm^{-2}V^{-1}s^{-1}$, resulting in great improvements of power factor. At the same time, Zn substitution decreased the lattice thermal conductivity due to the isoelectronic substitution introduced mass fluctuation scattering and strain field fluctuation scattering. The interplay between the Seebeck coefficient, the electrical resistivity, and the thermal conductivity of $Mg_2Si_{0.5}Sn_{0.49}Sb_{0.01}$ substituted with Zn results in an enhancement of the thermoelectric figure of merit by 25% at ~730 K, from $ZT \approx 0.8$ in $Mg_2Si_{0.5}Sn_{0.49}Sb_{0.01}$ to $ZT \approx 1.0$ in $Mg_{1.98}Zn_{0.02}Si_{0.5}Sn_{0.49}Sb_{0.01}$. This provides a new promising avenue for partially decoupling the interrelation electron and phonon transport, and eventually for optimizing thermoelectric properties.

Acknowledgements

References

1   D.M. Rowe, C.M. Bhandari, Modern thermoelectrics. Reston Publishing Company,

Inc. Reston, Virginia, 1996.

2   B. Poudel, Q. Hao, Y. Ma, Y.C. Lan, A. Minnich, B. Yu, X. Yan, D.Z. Wang, A. Muto, D. Vashaee, X.Y. Chen, J.M. Liu, M.S. Dresselhaus, G. Chen, Z.F. Ren, *Science*, 2008**, 320**, 634-638.

3   J.J. Shen, T.J. Zhu, X.B. Zhao, S.N. Zhang, S.H. Yang and Z.Z. Yin, *Energy Environ. Sci.*, 2010, **3**, 1519-1523.

4   J.P. Heremans, V. Jovovic, E.S. Toberer, A. Saramat, K. Kurosaki, A. Charoenphakdee, S. Yamanaka, G.J. Snyder, *Science*, 2008, **321**, 554-557.

5   K. Biswas, J.Q. He, I.D. Blum, C.I Wu, T.P. Hogan, D.N. Seidman, V.P. Dravid, M.G. Kanatzidis, *Nature*, 2012, **489**, 414-418.

6   X. Shi, J. Yang, J.R. Salvador, M.F. Chi, J.Y. Cho, H. Wang, S.Q. Bai, J.H. Yang, W.Q. Zhang and L.D. Chen, *J. Am. Chem. Soc.*, 2011, **133**, 7837-7846.

7   M.S. Dresselhaus, G. Chen, M.Y. Tang, R.G. Yang, H. Lee, D.Z. Wang, Z.F. Ren, J.P. Fleurial and P. Gogna, *Adv. Mater.*, 2007, **19**, 1043-1053.

8   Y.C. Lan, A.J. Minnich, G. Chen, Z.F. Ren, *Adv. Funct. Mater*, 2009, **19**, 1-20.

9   Y.Z. Pei, H. Wang, G.J. Snyder, *Adv. Mater.*, 2012, **24**, 6125-6135.

10   J.P. Heremans, B. Wiendlocha, A.M. Chamoire, *Energy Environ. Sci.*, 2012, **5**, 5510-5530.

11   V.K. Zaitsev, M.I. Fedorov, E.A. Gurieva, I.S. Eremin, P.P. Konstantinov, A.Y. Samunin, M.V. Vedernikov, *Phys. Rev. B*, 2006, **74**, 045207.

12   Q. Zhang, J. He, T.J. Zhu, S.N. Zhang, X.B. Zhao, T.M. Tritt, *Appl. Phys. Lett.*, 2008, **93**, 102109.

13   W. Liu, X.J. Tan, K. Yin, H.J. Liu, X.F. Tang, J. Shi, Q.J. Zhang, C. Uher, *Phys. Rev.*

Lett., 2012, **108**, 166601.

14 H.L. Gao, T.J. Zhu, X.X. Liu, L.X. Chen, X.B. Zhao, *J. Mater. Chem.*, 2011, **21**, 5933-5937.

15 W. Liu, X.F. Tang, H. Li, J. Sharp, X.Y. Zhou, C. Uher, *Chem. Mater.*, 2011**, 23**, 5256-5263.

16 Y. Isoda, T. Nagai, H. Fujiu, Y. Imai, Y. Shinohara, *International Conference on Thermoelectric*, 2006, 406-410.

17 Z.L. Du, T.J. Zhu, Y. Chen, J. He, H.L. Gao, G.Y. Jiang, T.M. Tritt, X.B. Zhao, *J. Mater. Chem.*, 2012, **22**, 6838-6844.

18 Y. Isoda, T. Nagai, H. Fujiu, Y. Imai, Y. Shinohara, *International Conference on Thermoelectrics*, 2007, 251-255.

19 Q. Zhang, J. He, X.B. Zhao, S.N. Zhang, T.J. Zhu, H. Yin, T.M. Tritt, *J. Phys. D: Appl. Phys*., 2008, **41**, 185103.

20 J.I. Tani, H. Kido, *J. Alloy Compd.*, 2008, **466**, 335-340.

21 X.H. Liu, T.J. Zhu, H. Wang, L.P. Hu, H.H. Xie, G.Y. Jiang, G.J. Snyder, X.B. Zhao, *Adv. Energy Mater.*, 2013, **3**, 1238-1244.

22 G.S. Nolas, D. Wang, M. Beekman, *Phys. Rev. B*, 2007, **76**, 235204.

23 T. Dasgupta, C. Stiewe, R. Hassdorf, A.J. Zhou, L. Boettcher, E. Mueller, *Phys. Rev. B*, 2011, **83**, 235207.

24 P. Zwolenski, J. Tobola, S. Kaprzyk, *J. Electron. Mater.*, 2011, **40**, 889-897.

25 J. Singh, P. Kumar, K.S. Hui, K.N. Hui, K. Ramam, R.S. Tiwaria, O.N. Srivastava, *CrystEngComm*, 2012**, 14**, 5898-5904.

26 Z.M. Gibbs, A. LaLonde, G.J. Snyder, *New J. Phys.*, 2013, **15**, 075020.

27 M.I. Fedorov, V.K. Zaitsev, G.N. Isachenko, *Solid State Phenomena*, 2011, **170**, 286-292.

28 A.F. May, J.P. Fleurial, G.J. Snyder, *Phys. Rev. B*, 2008, **78**, 125205.

29 J.J. Pulikkotil, D.J. Singh, S. Auluck, M. Saravanan, D.K. Misra, A. Dhar, R.C. Budhani, *Phys. Rev. B*, 2012, **86**, 155204.

30 D.G. Cahill, S.K. Watson, R.O. Pohl, *Phys. Rev. B*, 1992, **46**, 6131-6140.

31 A. Zevalkink, Y. Takagiwa, K. Kitahara, K. Kimurab, G.J. Snyder, *Dalton Trans.*, 2014, **43**, 4720-4725.

32 C. Yu, T. J. Zhu, R. Z. Shi, Y. Zhang, X. B. Zhao and J. He, *Acta Mater.*, 2009, **57**, 2757-2764.

Figure captions:

Fig. 1 X-ray diffraction patterns of as-hot-pressed pellets of $Mg_{2-x}Zn_xSi_{0.5}Sn_{0.5}$ and $Mg_{2-y}Zn_ySi_{0.5}Sn_{0.49}Sb_{0.01}$ samples.

Fig. 2 Temperature dependences of (a) the electrical conductivity σ (b) the Seebeck coefficient α of as-hot-pressed pellets of $Mg_{2-x}Zn_xSi_{0.5}Sn_{0.5}$ and $Mg_{2-y}Zn_ySi_{0.5}Sn_{0.49}Sb_{0.01}$ samples.

Fig. 3 Room temperature carrier concentration n and mobility μ_H vs Zn content.

Fig. 4 Room temperature carrier concentration dependence of Seebeck coefficient of $Mg_2Si_{0.5}Sn_{0.5}$ based thermoelectric materials. Black square represents data of this work; red circle represents data from W. Liu et $al.$ [15]; blue triangle represents data from H.L. Gao et $al.$ [14].

Fig. 5 Temperature dependences of (a) total thermal conductivity κ, (b) Lorenz number L, (c) lattice thermal conductivity κ_L of $Mg_{2-y}Zn_ySi_{0.5}Sn_{0.49}Sb_{0.01}$ samples.

Fig. 6 (a) Temperature dependences of ZTs of $Mg_{2-y}Zn_ySi_{0.5}Sn_{0.49}Sb_{0.01}$ samples, (b) ZT values at 750 K as a function of carrier concentration of $Mg_2Si_{0.5}Sn_{0.5}$ based thermoelectric materials.

Table of contents entry:

Isoelectronic Zn substitution in $Mg_2Si_{0.5}Sn_{0.5}$ based thermoelectric materials improved mobility without affecting carrier concentration, leading to an enhancement of *ZT*.
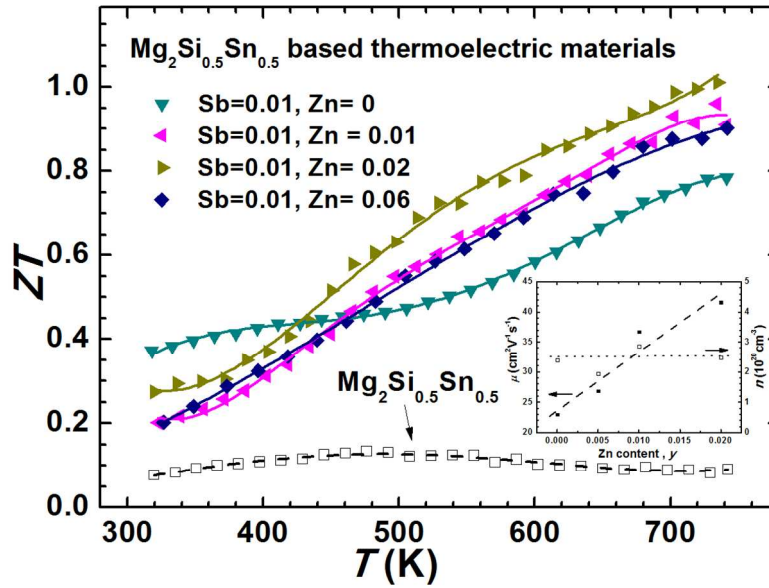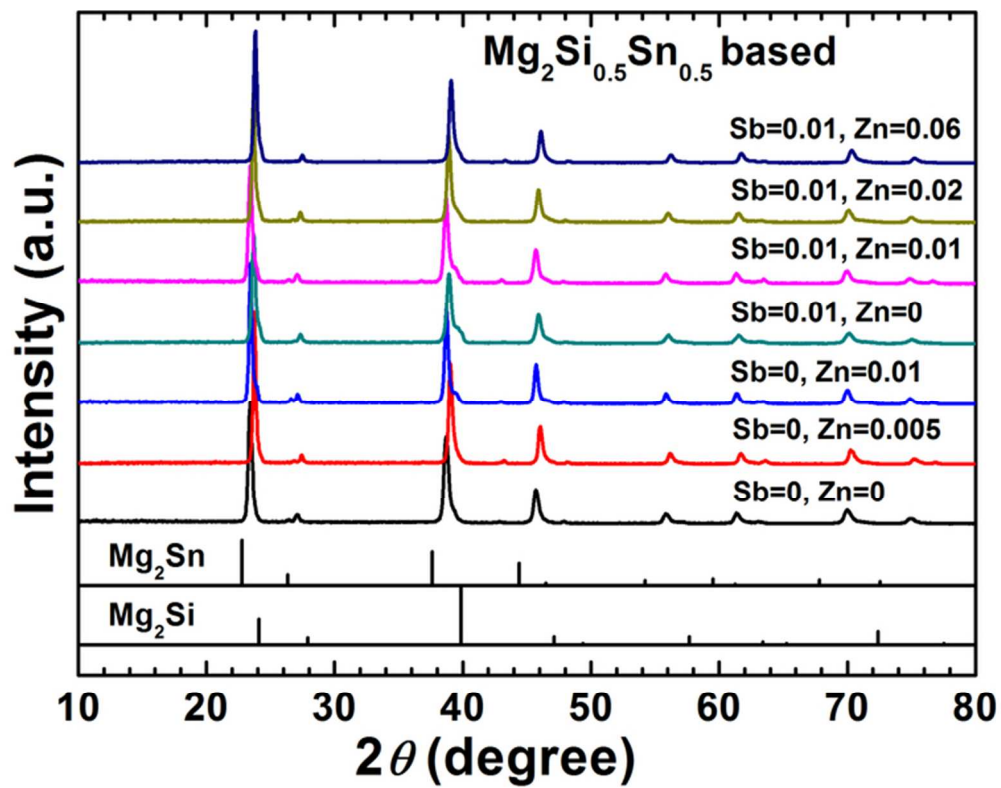
Fig. 1 X-ray diffraction patterns of as-hot-pressed pellets of Mg2-xZnxSi0.5Sn0.5 and Mg2-yZnySi0.5Sn0.49Sb0.01 samples.
64x49mm (300 x 300 DPI)
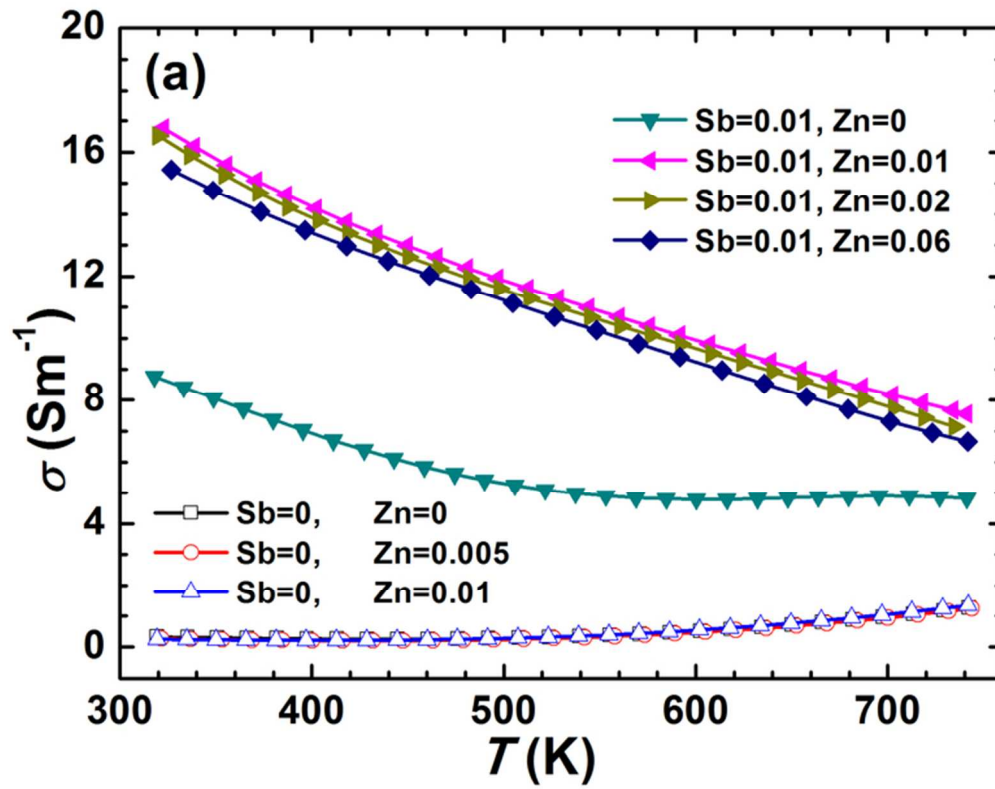
Fig. 2(a) Temperature dependences of the electrical conductivity of as-hot-pressed pellets of Mg2-xZnxSi0.5Sn0.5 and Mg2-yZnySi0.5Sn0.49Sb0.01 samples.
65x51mm (300 x 300 DPI)
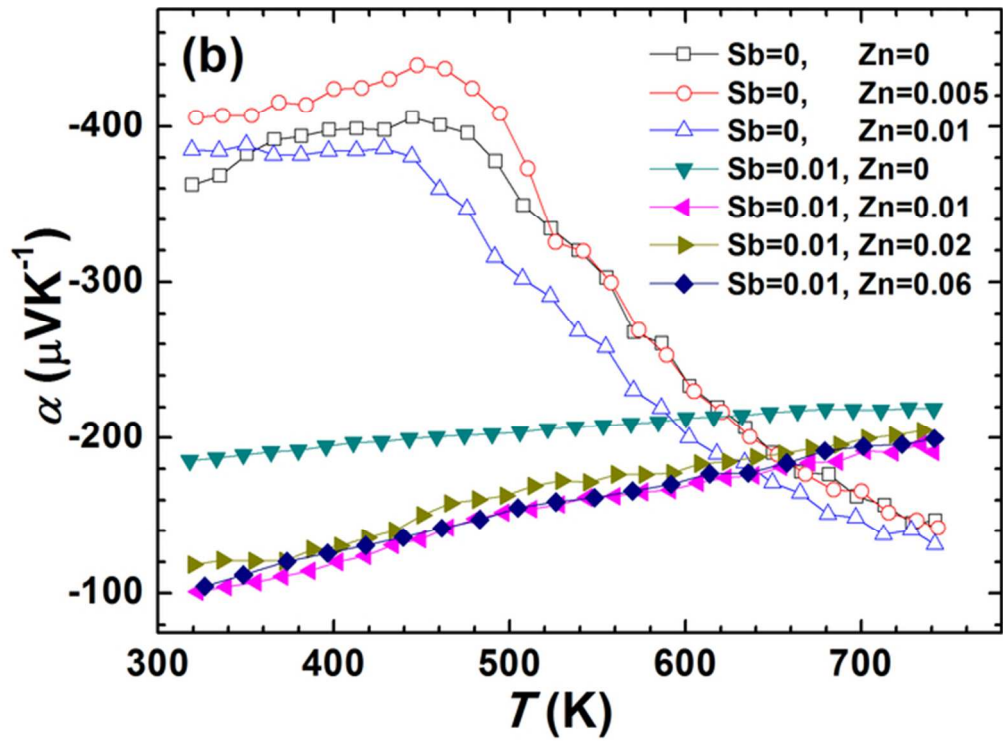
Fig. 2(b) Temperature dependences of the Seebeck coefficient of as-hot-pressed pellets of Mg2-xZnxSi0.5Sn0.5 and Mg2-yZnySi0.5Sn0.49Sb0.01 samples.
60x44mm (300 x 300 DPI)
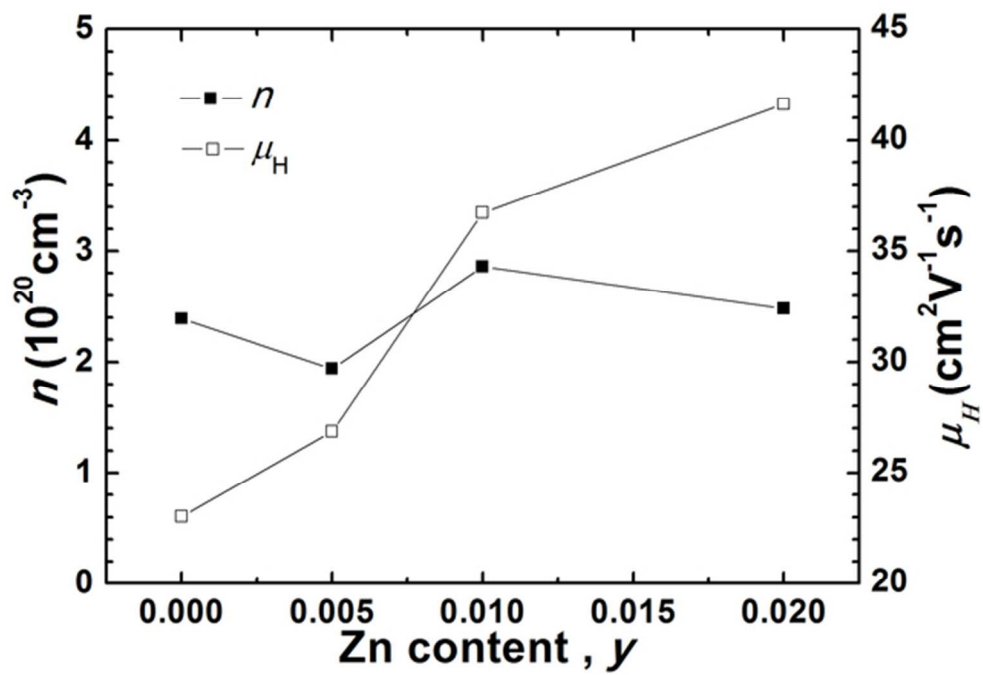
Fig. 3 Room temperature carrier concentration n and mobility μH vs Zn content.
55x37mm (300 x 300 DPI)
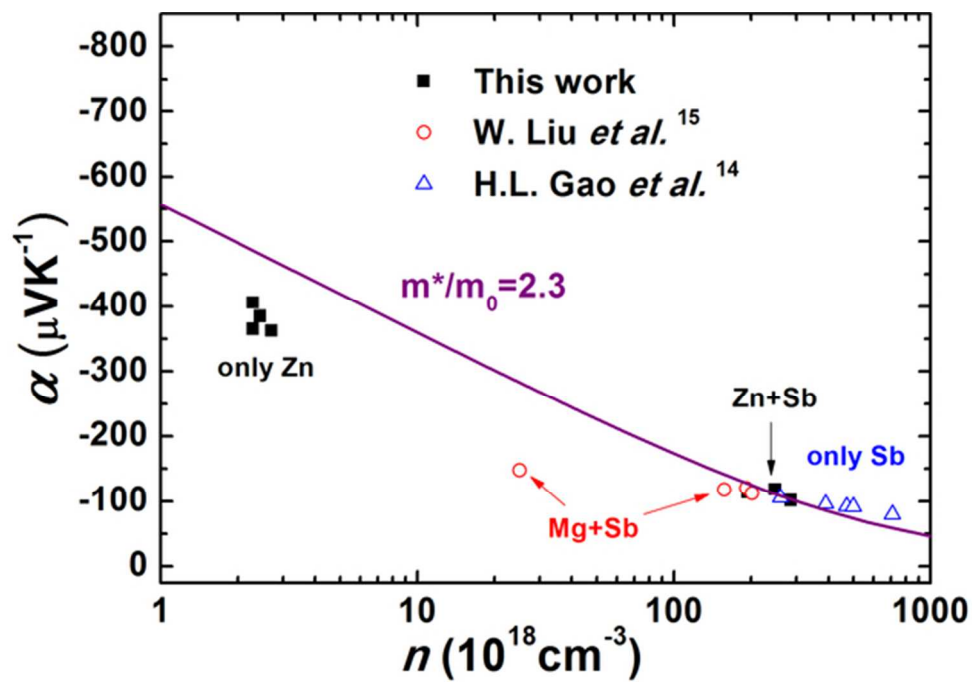
Fig. 4 Room temperature carrier concentration dependence of Seebeck coefficient of Mg2Si0.5Sn0.5 based thermoelectric materials. Black square represents data of this work; red circle represents data from W. Liu et al. 15; blue triangle represents data from H.L. Gao et al. 14.
55x37mm (300 x 300 DPI)
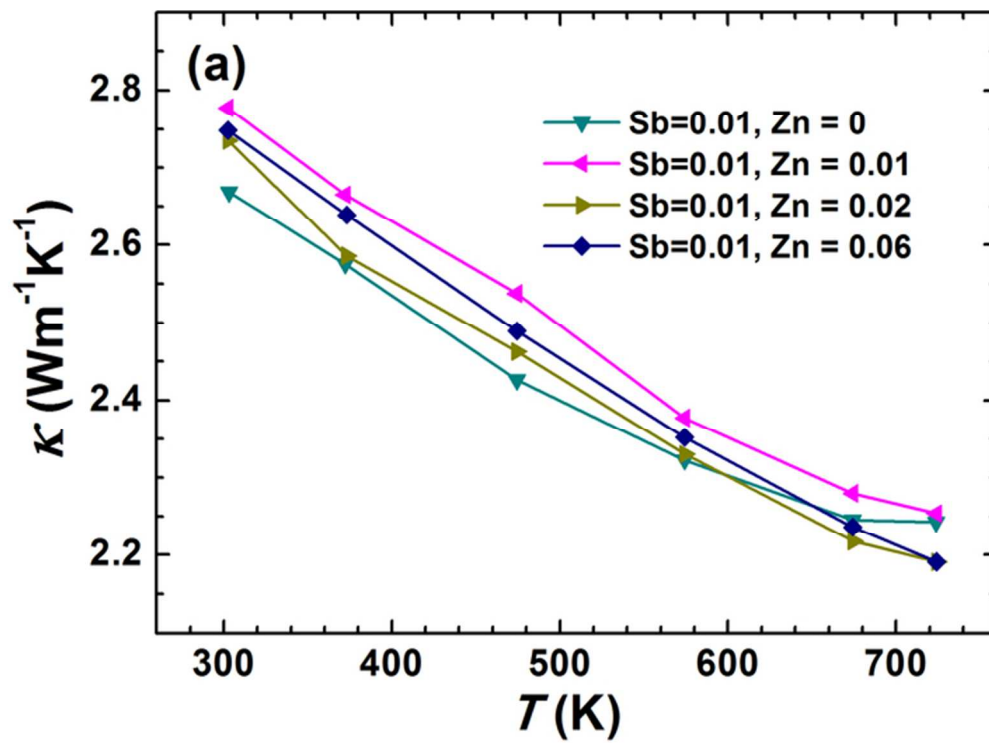
Fig 5(a) Temperature dependences of total thermal conductivity κ of Mg2-yZnySi0.5Sn0.49Sb0.01 samples.
60x44mm (300 x 300 DPI)
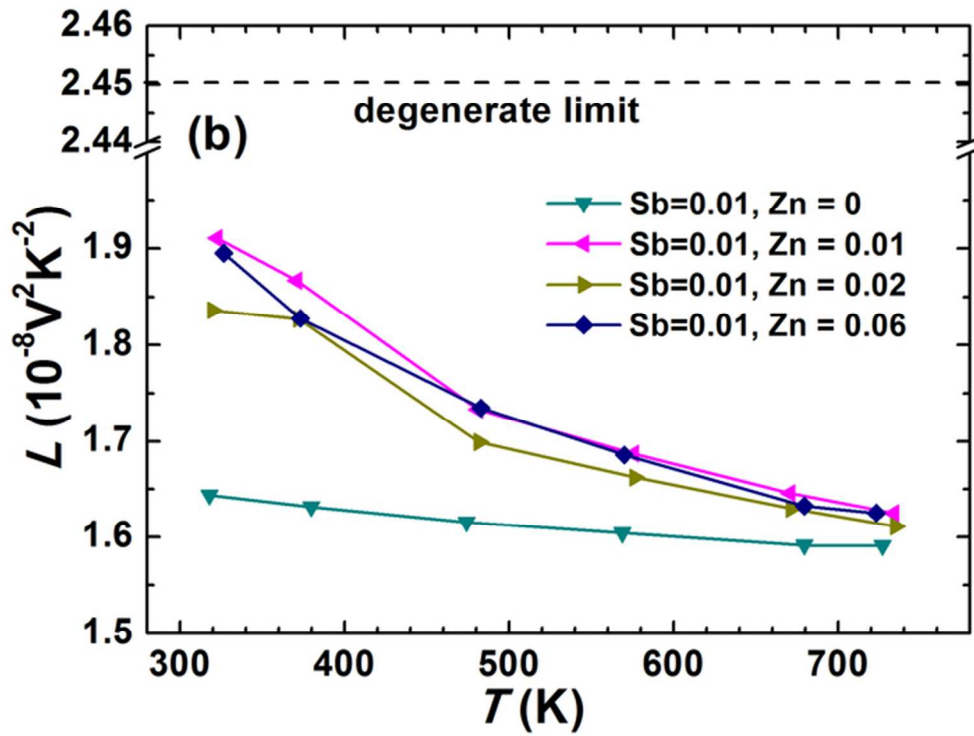
Fig. 5(b) Temperature dependences of Lorenz number L of Mg2-yZnySi0.5Sn0.49Sb0.01 samples.
60x44mm (300 x 300 DPI)
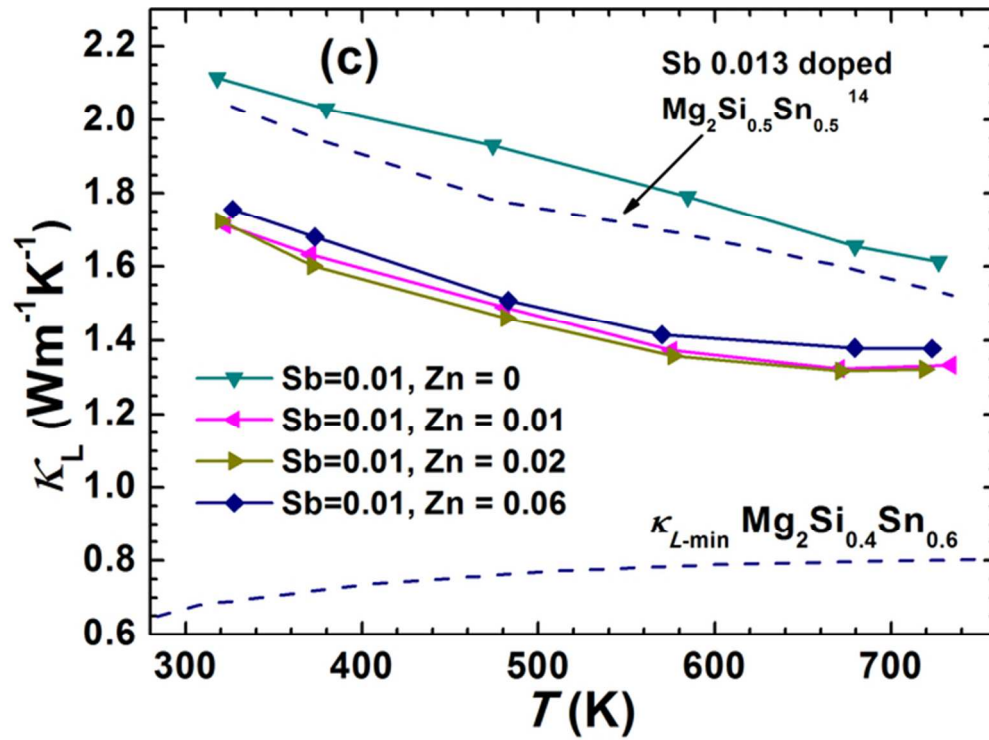
Fig. 5(c) Temperature dependences of lattice thermal conductivity κL of Mg2-yZnySi0.5Sn0.49Sb0.01 samples.
60x44mm (300 x 300 DPI)
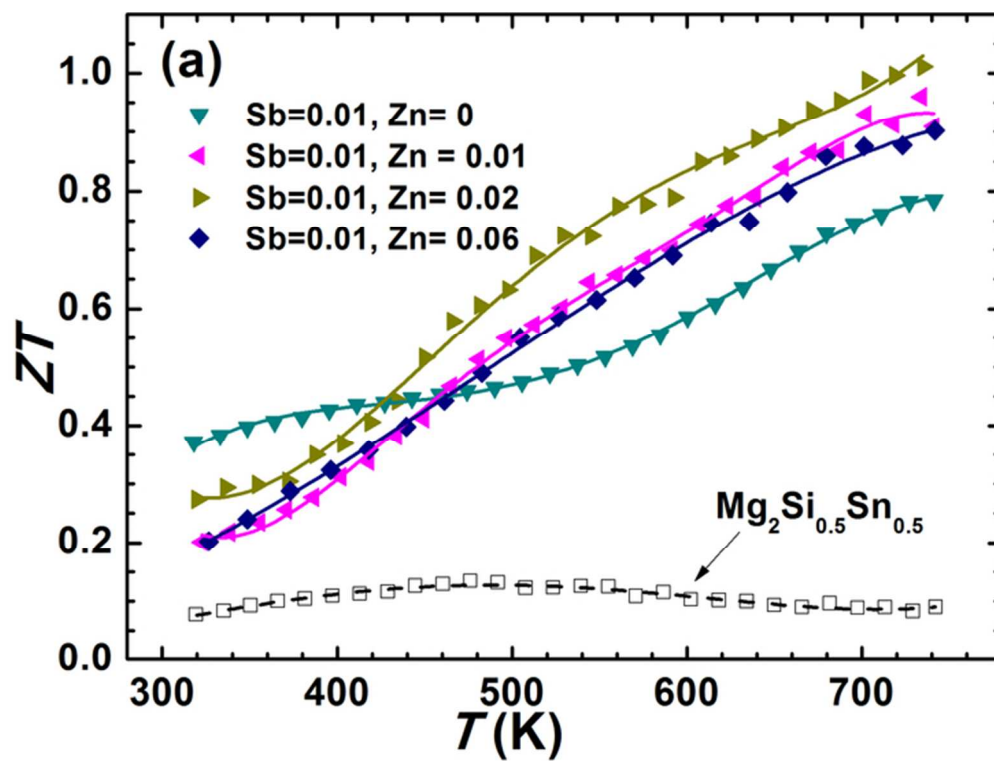
Fig. 6(a) Temperature dependences of ZTs of Mg2-yZnySi0.5Sn0.49Sb0.01 samples
61x46mm (300 x 300 DPI)
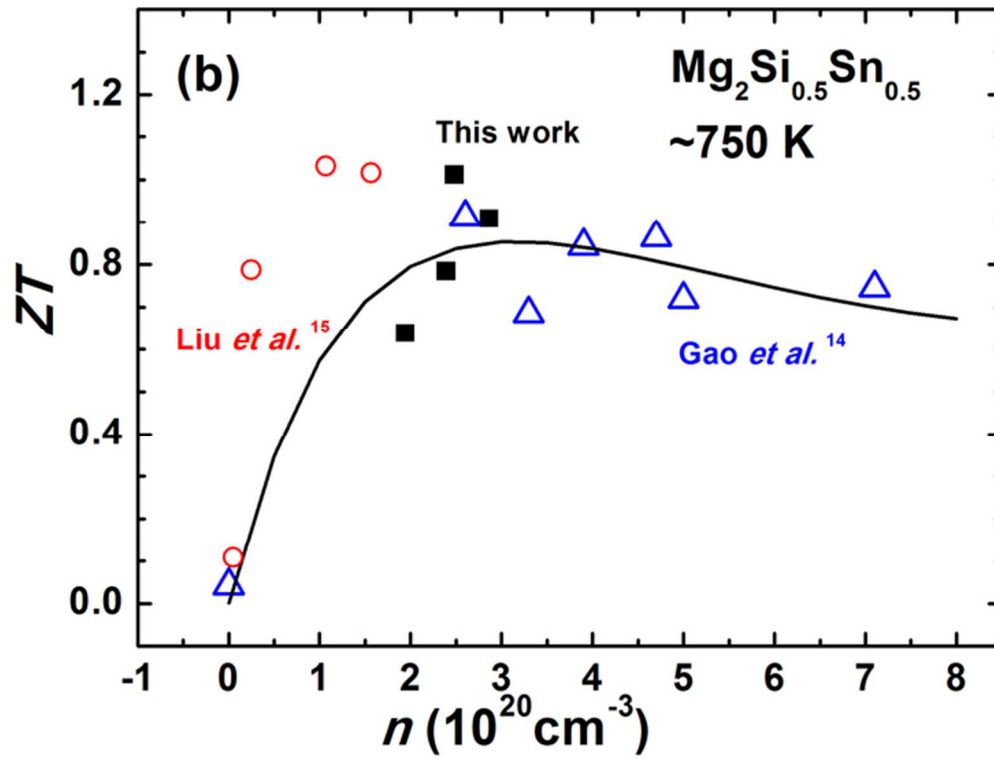
Fig. 6(b) ZT values at 750 K as a function of carrier concentration of Mg2Si0.5Sn0.5 based thermoelectric materials.
61x46mm (300 x 300 DPI)